

PROPERTIES AND EVOLUTION OF THE REDBACK MILLISECOND PULSAR BINARY PSR J2129–0429

ERIC C. BELLM^{1,2}, DAVID L. KAPLAN³, RENE P. BRETON^{4,5}, E. STERL PHINNEY¹, VARUN B. BHALERAO⁶, FERNANDO CAMILO⁷, SUMIT DAHAL⁸, S. G. DJORGOVSKI¹, ANDREW J. DRAKE¹, J. W. T. HESSELS^{9,10}, RUSS R. LAHER¹¹, DAVID B. LEVITAN¹, FRASER LEWIS^{12,13}, ASHISH A. MAHABAL¹, ERAN O. OFEK¹⁴, THOMAS A. PRINCE¹, SCOTT M. RANSOM¹⁵, MALLORY S. E. ROBERTS¹⁶, DAVID M. RUSSELL⁸, BRANIMIR SESAR¹⁷, JASON A. SURACE¹¹, SUMIN TANG¹

Submitted to ApJ

ABSTRACT

PSR J2129–0429 is a “redback” eclipsing millisecond pulsar binary with an unusually long 15.2 hour orbit. It was discovered by the Green Bank Telescope in a targeted search of unidentified Fermi gamma-ray sources. The pulsar companion is optically bright (mean $m_R = 16.6$ mag), allowing us to construct the longest baseline photometric dataset available for such a system. We present ten years of archival and new photometry of the companion from LINEAR, CRTS, PTF, the Palomar 60-inch, and LCOGT. Radial velocity spectroscopy using the Double-Beam Spectrograph on the Palomar 200-inch indicates that the pulsar is massive: $1.74 \pm 0.18 M_\odot$. The G-type pulsar companion has mass $0.44 \pm 0.04 M_\odot$, one of the heaviest known redback companions. It is currently $95 \pm 1\%$ Roche-lobe filling and only mildly irradiated by the pulsar. We identify a clear $13.1 \text{ mmag yr}^{-1}$ secular decline in the mean magnitude of the companion as well as smaller-scale variations in the optical lightcurve shape. This behavior may indicate that the companion is cooling. Binary evolution calculations indicate that PSR J2129–0429 has an orbital period almost exactly at the bifurcation period between systems that converge into tighter orbits as black widows and redbacks and those that diverge into wider pulsar–white dwarf binaries. Its eventual fate may depend on whether it undergoes future episodes of mass transfer and increased irradiation.

Subject headings: pulsars: individual (PSR J2129–0429)

1. INTRODUCTION

Millisecond pulsars (MSPs) eclipsed by material from their low-mass binary companions may provide a major

¹ Cahill Center for Astronomy and Astrophysics, California Institute of Technology, Pasadena, CA 91125

² ebllm@caltech.edu

³ Department of Physics, University of Wisconsin-Milwaukee, Milwaukee, WI 53201, USA

⁴ Jodrell Bank Centre for Astrophysics, Alan Turing Building, School of Physics and Astronomy, The University of Manchester, Oxford Road, Manchester, M13 9PL, U.K.

⁵ School of Physics and Astronomy, University of Southampton, Southampton, SO17 1BJ, U.K.

⁶ Inter University Centre for Astronomy and Astrophysics, PO Bag 4, Ganeshkhind, Pune 411007, India

⁷ Columbia Astrophysics Laboratory, Columbia University, New York, NY 10027, USA

⁸ New York University Abu Dhabi, PO Box 129188, Abu Dhabi, UAE

⁹ ASTRON, the Netherlands Institute for Radio Astronomy, Postbus 2, 7990 AA, Dwingeloo, The Netherlands

¹⁰ Anton Pannekoek Institute for Astronomy, University of Amsterdam, Science Park 904, 1098 XH Amsterdam, The Netherlands

¹¹ Infrared Processing and Analysis Center, California Institute of Technology, Pasadena, CA 91125

¹² Faulkes Telescope Project, School of Physics and Astronomy, Cardiff University, 5 The Parade, Cardiff, CF24 3AA, Wales, UK

¹³ Astrophysics Research Institute, Liverpool John Moores University, IC2, Liverpool Science Park, 146 Brownlow Hill, Liverpool L3 5RF, UK

¹⁴ Benozio Center for Astrophysics, Faculty of Physics, Weizmann Institute of Science, Rehovot 76100, Israel

¹⁵ National Radio Astronomy Observatory, 520 Edgemont Road, Charlottesville, Virginia 22903-2475, USA

¹⁶ Eureka Scientific Inc., 2452 Delmer Street, Suite 100, Oakland, California 94602-3017, USA

¹⁷ Max Planck Institute for Astronomy, Königstuhl 17, D-69117 Heidelberg, Germany

path to the production of isolated MSPs: after spinning up the pulsar through accretion (Alpar et al. 1982; Radhakrishnan & Srinivasan 1982; Bhattacharya & van den Heuvel 1991), the pulsar wind may ablate away the donor (van den Heuvel & van Paradijs 1988; Phinney et al. 1988; Kluzniak et al. 1988). This cannibalism suggested the name “Black Widow” upon the discovery of the first example, which had a companion mass of only a few percent M_\odot (Fruchter et al. 1988). Later observations and theoretical work suggested that the ablation rate for the first Black Widow system might be too slow to evaporate its companion in a Hubble time, however (Levinson & Eichler 1991; Fruchter & Goss 1992). Ablation may be more efficient in other systems (e.g., Bailes et al. 2011), such that the companion is completely destroyed or only a small remnant remains. Instabilities in very low mass companions (Deloye & Bildsten 2003) or dynamical encounters in globular clusters (King et al. 2003) provide alternative means to produce isolated MSPs.

Today, thanks to targeted radio and X-ray surveys of globular clusters and, more recently, in regions of the broader Galactic Field where *Fermi*-LAT has localized sources, more than 30 black widow systems are known (Roberts 2013, and references therein). Moreover, many “redback” systems¹⁸ with higher-mass, non-degenerate companions of $0.2\text{--}0.7 M_\odot$ have been discovered (Roberts 2013, and references therein; Crawford et al. 2013). The discovery of several redback systems that transition between accretion-powered low-mass X-ray binary states and rotation-powered radio pulsar states has provided further support for the recycling scenario (Archibald

¹⁸ Redback spiders are the Australian cousins of Black Widow spiders.

et al. 2009; Papitto et al. 2013; Bassa et al. 2014; Stappers et al. 2014; Patruno et al. 2014). Irradiation feedback and accretion disk instabilities may be responsible for the relatively short timescale transitions (years) observed between accreting and detached states (Benvenuto et al. 2015). Current models disagree as to whether redbacks and black widows are distinct populations that evolve separately due to bimodal evaporation efficiency (Chen et al. 2013) or whether black widow systems are an endpoint in the evolution of some redback systems (Benvenuto et al. 2014).

In the optical bands, black widow and redback binaries show large-amplitude variability due to effects such as the ellipsoidal modulation of the near-Roche filling companion, dayside and nightside temperature differentials, and gravity darkening. The apparent magnitudes of these systems vary considerably with distance and the intrinsic luminosity of their companions. With their larger companions and relative proximity, redbacks in the Galactic Field are the brightest of these systems in the optical band, allowing for detailed photometric and spectroscopic monitoring with moderate aperture telescopes (e.g., Breton et al. 2013; Li et al. 2014; Schroeder & Halpern 2014). MSP binaries in the Field are also useful tracers of binary evolution, as unlike systems in globular clusters they are unlikely to experience dynamical exchange encounters.

With a radio timing solution and an optical radial velocity amplitude from the companion, it is possible to measure the mass ratio of the pulsar and its companion. While expected theoretically (e.g., Phinney & Kulkarni 1994; Benvenuto et al. 2014), the neutron star masses in the black widow and redback systems measured to date have largely proven to be heavier than $1.4 M_{\odot}$ (van Kerkwijk et al. 2011; Romani et al. 2012; Deller et al. 2012; Crawford et al. 2013). Measurement of pulsar masses in these systems thus provides a valuable expansion of the sample needed to understand the recycling process. While the most precise measurements of the masses of high-mass neutron stars have been obtained through measurement of Shapiro delay (Nice et al. 2005; Demorest et al. 2010; Freire et al. 2011), discovery of additional heavy neutron stars in pulsar binaries of various types (e.g., Bassa et al. 2006; Kaplan et al. 2013; Antoniadis et al. 2013; Strader et al. 2015) can also inform studies of the equation of state of neutron stars (for a review, see Lattimer 2012).

PSR J2129–0429 is a redback system with a bright (mean $m_R = 16.6$) optical counterpart. The gamma-ray counterpart to PSR J2129–0429 appeared in the first *Fermi* source catalog as 1FGL J2129.8–0427 (Abdo et al. 2010) and in subsequent versions as 2FGL J2129.8–0428 (Nolan et al. 2012) and 3FGL J2129.6–0427 (The Fermi-LAT Collaboration 2015). The *Fermi* spectrum does not show significant curvature, making it difficult to firmly classify as a pulsar based on the gamma-ray data alone (e.g., Ackermann et al. 2012).

Nevertheless, a radio survey of the 1FGL error box with the Green Bank Telescope identified a pulsar counterpart with a spin period of 7.62 ms (Hessels et al. 2011). The dispersion measure of 16.9 pc cm^{-3} implies a distance of 0.9 kpc using the NE2001 model (Cordes & Lazio 2002). Phase-folded X-ray observations of the system

show an unusual double-peaked phase profile from the intra-binary shock, suggesting a compact but structured emission region (Roberts et al. 2015).

In this paper we present optical photometry and spectroscopy of the PSR J2129–0429 binary system. In §2 we describe the observations. We perform fits to the radial velocity amplitude in §3 and to the system geometry in §4. In §5 we present evidence for secular evolution in the lightcurve. We close with a discussion of the evolution of PSR J2129–0429 (§6).

Throughout the paper, we use the convention that the zero point of orbital phase occurs when the companion is between the pulsar and the Earth (companion inferior conjunction). The Time of Ascending Node is accordingly at phase 0.75 in this convention.

2. OBSERVATIONS

2.1. Photometry

Using the localization of PSR J2129–0429 provided by a preliminary radio-derived pulsar timing ephemeris (21h29m45.039±0.001s, $-04^{\circ}29'05.59 \pm 0.08''$ (J2000); Bangale et al., in prep), we found a bright ($m_R \sim 16.5$) optical counterpart in the databases of several time-domain surveys that varied at the orbital period of 15.245 hr. We also acquired new multicolor phase-resolved observations to enable detailed lightcurve modeling.

The optical counterpart of PSR J2129–0429 was repeatedly detected in imaging conducted by the Palomar Transient Factory (PTF) (Law et al. 2009; Rau et al. 2009) on the Palomar Samuel Oschin 48-inch Schmidt (P48) at 21h29m45.06s, $-04^{\circ}29'06.8''$ (J2000)¹⁹. We obtained calibrated aperture photometry for PSR J2129–0429 from the standard PTF photometric pipeline, which includes image reduction (Laher et al. 2014), photometric calibration (Ofek et al. 2012) to the Sloan Digital Sky Survey (York et al. 2000), and a relative photometry correction for each image to remove any residual scalar offsets in the zero-points due to non-photometric conditions (c.f. Ofek et al. 2011, Appendix A). We added a systematic error of 0.01 mag in quadrature with the pipeline-generated photometric errors so that a constant fit to a nearby (53.6'' separation) comparison star (21h29m46.9s, $-04^{\circ}28'20.5''$, $m_R = 16.6$ mag) had reduced chi-squared $\chi^2_{\nu} = 1$.

PSR J2129–0429 is also present in data from the Catalina Real-time Transient Survey (CRTS; Drake et al. 2009) catalog and in its associated catalog of periodic sources (Drake et al. 2014). The Catalina images are spaced ten minutes apart to look for asteroid motion. The magnitudes are obtained by running SExtractor (Bertin & Arnouts 1996) on the images and then calibrating them to the V band²⁰, as the raw CCD images

¹⁹ Typical PTF absolute astrometric errors are 0.1–0.2'' RMS. The 1.25'' distance of the radio position may be due to covariances between the orbital derivatives and spindown in the relatively short radio timing baseline. The SDSS DR12 (Alam et al. 2015) position of the object (21h29m45.05s, $-04^{\circ}29'06.83''$) is consistent with the PTF position.

²⁰ More details for the CRTS Second Data Release (DR2) magnitudes can be found at <http://nesssi.cacr.caltech.edu/DataRelease/FAQ2.html#calib>. The set of observations used here included dates outside the DR2 release. Magnitudes from these observations are taken from the transient pipeline and lack the small

are unfiltered.

Additionally, the system was imaged by the Lincoln Near-Earth Asteroid Research survey (LINEAR; Stokes et al. 2000; Sesar et al. 2011). We performed PSF photometry on the images and photometrically calibrated the images to SDSS.

We acquired targeted phase-resolved observations of PSR J2129–0429 in g' , r' , and i' using the CCD camera on the roboticized Palomar 60-inch telescope (P60; Cenko et al. 2006) between November 2011 and June 2012. Basic image reductions were performed by the automated pipeline. We obtained aperture photometry for the source and companion stars using SExtractor and calibrated the photometry to SDSS.

We obtained additional g' , r' , i' and z' imaging of PSR J2129–0429 using the Las Cumbres Observatory Global Telescope (LCOGT) Network over a period of a month starting 26 October 2014. Observations were made using the 1-m LCOGT network sites at Siding Spring Observatory, Australia, Cerro Tololo Inter-American Observatory, Chile, McDonald Observatory, USA and SAAO, South Africa, as well as the 2-m Faulkes Telescopes at Haleakala Observatory, Maui, Hawaii, USA and Siding Spring Observatory, Australia. The data reduction was performed using LCOGT’s automatic pipeline and aperture photometry was conducted with IRAF version 2.16.1 (Tody 1986) and calibrated to SDSS using four bright, unsaturated stars visible in all images.

All times were corrected to the Solar System barycenter. The photometric observations are summarized in Table 1.

2.2. Spectroscopy

We obtained spectra of PSR J2129–0429 using the Palomar 200-inch Hale telescope and the Double-Beam Spectrograph (DBSP; Oke & Gunn 1982) using the new red camera (Rahmer et al. 2012). Table 2 lists the observation parameters. We reduced data from both arms of the spectrograph using a custom PyRAF-based pipeline²¹. The pipeline performs standard image processing and spectral reduction procedures, including bias subtraction, flat-field correction, wavelength calibration, optimal spectral extraction, and flux calibration. To account for instrument flexure in individual science spectra, we subtract an average wavelength offset computed from known sky lines on a per-frame basis (Sesar et al. 2013). The RMS scatter of the corrected sky line positions provides an estimate of the uncertainty in the wavelength solution, which we add in quadrature with the template fitting uncertainty when computing radial velocities (Section 3). The mean uncertainty for these observations was 6.2 km s^{-1} at 4750 \AA on the blue side and 8.6 km s^{-1} at 7400 \AA on the red side. Figures 1 and 2 show the reduced spectra ordered by pulsar orbital phase.

The spectra indicate that the companion of PSR J2129–0429 is non-degenerate, with features resembling a G-type star. Some variation in the line strengths is observed. From the few observations we have that are repeated near phase 0, there appears to be stochastic variability in addition to phase-dependent

differences (Figures 1 and 2).

3. RADIAL VELOCITY

We obtained radial velocity measurements from our spectra using a template-fitting approach as implemented in Bhalerao et al. (2012). We fit flux-calibrated spectra with the stellar atmosphere models of Munari et al. (2005), using a linear polynomial to account for any residual fluxing errors. We included an extinction coefficient of $A_V = 0.10 \text{ mag}$ (Schlafly & Finkbeiner 2011). We fit the red-arm data from $5700\text{--}8900 \text{ \AA}$, omitting telluric bands at $6860\text{--}7000 \text{ \AA}$, $7570\text{--}7700 \text{ \AA}$, $7150\text{--}7350 \text{ \AA}$, and $8100\text{--}8400 \text{ \AA}$. The best-fit atmosphere model at all phases had $T = 5750 \text{ K}$, $\log g = 5.0$, solar metallicity, and 100 km s^{-1} rotational broadening. (These values are broadly consistent with the values we derive from binary modeling in Section 4 and our assumption of corotation.) By stepping the model through a grid of wavelength offsets, we determined the radial velocity at each epoch. A quadratic fit to the χ^2 surface provided 1σ error estimates, which we added in quadrature with the wavelength calibration uncertainties obtained in Section 2.2. Finally, we converted the observed radial velocities to the Solar System barycenter using Python routines derived from the Standards of Fundamental Astronomy Library (Board 2015). The χ^2/dof for the fit is 11.6/11. Figure 3 shows the resulting radial velocities and best-fit radial velocity amplitude using the radio ephemeris ($P_{\text{orb}} = 0.63522741310 \pm 3.3 \times 10^{-10} \text{ days}$; $TASC = 55702.111161463 \pm 9.8 \times 10^{-8}$)²² We find a radial velocity amplitude $K = 250.0 \pm 3.7 \text{ km s}^{-1}$. Together with the measured projected semi-major axis (1.85 lt-sec) from pulsar timing we find a mass ratio $q = 3.93 \pm 0.06$. Because the irradiation of the companion by the pulsar is modest and the mass ratio less extreme than in black widow systems (e.g., van Kerkwijk et al. 2011), the correction of the measured center of light RV amplitude to the center of mass is small ($\sim 0.2\%$), removing a potential source of systematic error. We nevertheless model this correction self-consistently in our binary fitting in the next section.

4. BINARY FITTING

We fit the available multicolor photometry from P60, and LCOGT as well as the 2009–2010 PTF data to a model of a distorted, irradiated binary companion using Icarus (Breton et al. 2013). This fitting computed filter-dependent photometry for a companion including the effects of irradiation and ellipsoidal modulation, which enable us to constrain the inclination, the masses of the binary members, the distance, the degree of irradiation, etc. Our fitting made use of prior probability distributions on the distance, extinction, and radial velocity amplitude. The distance prior was based on the dispersion measure (DM) distance of 900 pc (Cordes & Lazio 2002) with a conservative estimated uncertainty of 50% ($\pm 450 \text{ pc}$). The radial velocity amplitude prior was based on the measured radial velocity amplitude as well as the pulsar’s projected semi-major axis, and we used

²² We do not include radio-derived orbital period derivatives because the time baseline for our optical data extends well beyond the radio timing interval, which would lead to significant extrapolation errors from the higher-order period derivatives.

frame offsets applied in DR2.

²¹ <https://github.com/ebellm/pyraf-dbsp>

Table 1
Summary of Photometric Observations

Telescope	Filter	Start Date	End Date	Exposure (s)	Number	Precision (mmag)
LINEAR	open	2003 May 30	2011 Oct. 29	3–18	470	30
CRTS	open	2005 May 12	2014 May 5	30	365	76
P48	Mould <i>R</i>	2009 Jun. 26	2014 Oct. 11	60	116	14
P60	<i>g'</i>	2011 Nov. 10	2012 Jun. 14	60, 120	41	26
P60	<i>r'</i>	2011 Nov. 10	2012 Jun. 14	60, 120	43	20
P60	<i>i'</i>	2011 Nov. 10	2012 Jun. 14	60, 120	50	18
LCOGT 1 & 2 m	<i>g'</i>	2014 Oct. 26	2014 Nov. 22	100–200	25	29
LCOGT 1 & 2 m	<i>r'</i>	2014 Oct. 26	2014 Nov. 22	100–200	25	20
LCOGT 1 & 2 m	<i>i'</i>	2014 Oct. 26	2014 Nov. 22	100–200	23	28
LCOGT 1 & 2 m	Pan-STARRS <i>Z</i>	2014 Oct. 26	2014 Nov. 22	100–200	13	69

Table 2
Summary of Spectroscopic Observations.

Date (UTC)	Epoch at Barycenter (TDB MJD)	Orbital Phase	Aperture (arcsec)	Exposure Time (s)
2011-12-27	55922.07355	0.02	1.0	900
2012-05-29	56076.45451	0.06	1.0	900
2012-07-15	56123.43948	0.02	1.0	600
2012-09-20	56190.20842	0.13	0.5	900
2012-09-20	56190.25525	0.21	0.5	900
2012-09-20	56190.30287	0.28	0.5	900
2012-09-21	56191.19072	0.68	0.5	500
2012-09-21	56191.24078	0.76	0.5	900
2012-09-21	56191.30869	0.86	0.5	900
2013-06-02	56445.45257	0.95	0.5	900
2013-07-04	56477.47904	0.36	1.5	900
2013-07-04	56477.48975	0.38	1.5	900
2013-07-04	56477.50047	0.40	1.5	900

Note. — All observations were conducted with the Double Beam Spectrograph of the Palomar 200-inch Hale Telescope. Gratings used were 600 lines/mm blazed at 4000 Å (blue side) and 316 lines/mm blazed at 7500 Å (red side) for all dates except 2013 July 4, when the 1200/5000 and 1200/7100 gratings were used.

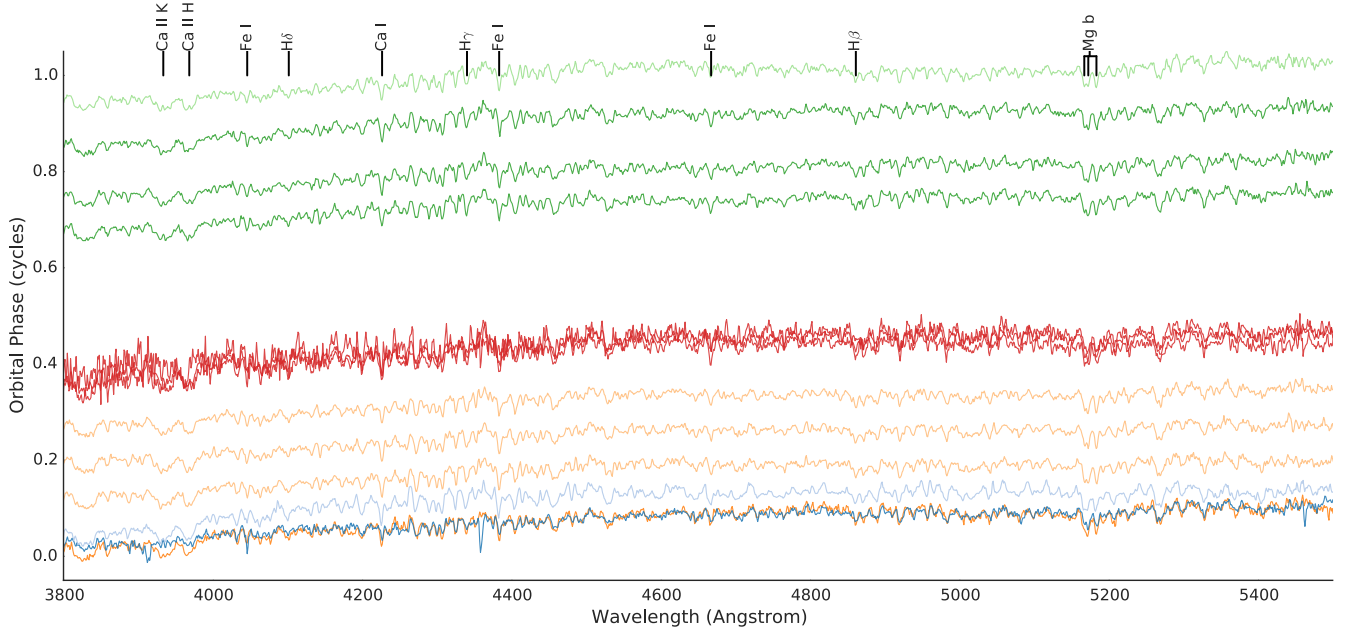


Figure 1. Blue-arm DBSP spectra of the PSR J2129–0429 companion ordered by pulsar orbital phase. Spectra are adjusted to zero velocity. Spectra obtained within one night of observing are plotted in the same color; Table 2 lists the orbital phase of each spectrum.

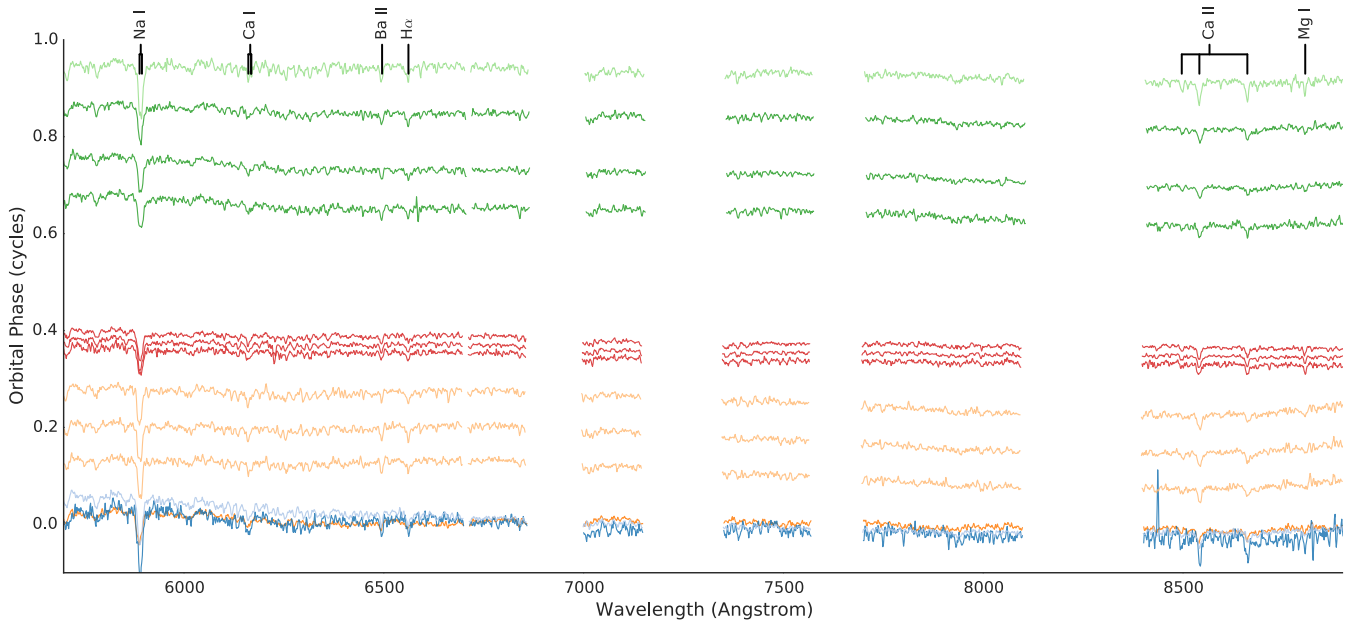


Figure 2. Red-arm DBSP spectra of the PSR J2129–0429 companion ordered by pulsar orbital phase. Colors are as in Figure 1. Regions of telluric absorption are masked, as is a small region near 6707 Å affected by a dome lamp fluorescence feature.

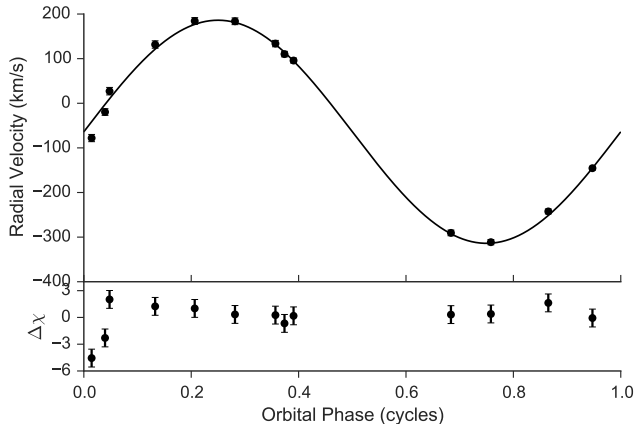


Figure 3. Radial velocity values, best-fit curve, and sigma residuals for PSR J2129–0429 from the DBSP red arm data. Error bars are comparable to the symbol size. The best fit amplitude is $K = 250.0 \pm 3.7 \text{ km s}^{-1}$ and the systemic velocity is $\gamma = -63.9 \pm 2.4 \text{ km s}^{-1}$.

$K = 250 \pm 4 \text{ km s}^{-1}$ as determined above. Finally we determined a prior on the extinction A_V based on the measured X-ray column density N_H and the observed $A_V(N_H)$ relation:

$$p(A_V) = 0.65\mathcal{N}(0.131, 0.082) + 0.35\mathcal{N}(0.068, 0.188) \quad (1)$$

(Roberts et al., in prep). Here, $\mathcal{N}(\mu, \sigma)$ represents a Gaussian probability distribution function (pdf) with mean μ and standard deviation σ ; both pdfs were properly truncated so that $A_V \geq 0$. Otherwise, we assumed flat priors on $\cos i$ (where i is the binary inclination), the nightside temperature T_{night} , the dayside temperature T_{day} , and the Roche-lobe filling factor f (here $f = R_{\text{nose}}/R_{L1}$ is the ratio of the radius of the companion pointing to the pulsar to that of the L1 point).

We performed a Markov-Chain Monte Carlo (MCMC) analysis of the photometry, fitting for $\cos i$, T_{night} , T_{day} , K , DM, A_V , and f , where $\text{DM} = -2.5 \log_{10}(d/10 \text{ pc})$ is the distance modulus. We included a 0.01 mag systematic uncertainty on each measurement, and we also allowed for individual offsets for each telescope/filter combination with an assumed zero-point uncertainty of 0.05 mag²³. Through these we could also determine the individual masses M_{NS} and M_c , the companion’s surface gravity $\log g$, as well as other related parameters such as the irradiation temperature T_{irr} (defined as $(T_{\text{day}}^4 - T_{\text{night}}^4)^{1/4}$), the irradiation efficiency η ($4\pi a^2 \sigma T_{\text{irr}}^4 / \dot{E}$), and the volume-averaged Roche-lobe filling factor R/R_L . We assumed corotation, although for a binary period of 15 hr the companion may not be tidally locked. We also assumed a gravity darkening coefficient $\beta = 0.08$ (with effective temperature $\propto g^\beta$ corresponding to a fully convective envelope; Lucy 1967). We used 192 individual walkers to explore the parameter space and followed each for 20,000 iterations. We then rejected the first 200 iterations as “burn-in”, and only included every 173rd point (based on observed autocorrelation lengths of 80–180 iterations for individual parameters). The results of the

²³ These normalization offsets remove the largest observed source of secular variation (§5). The fits are dominated by the P60 data, taken in 2011–2012. Little color or shape evolution is apparent in the more sparsely sampled 2014 LCOGT data.

MCMC are shown in Figure 4 and given in Table 3, where we list the mean of the posterior pdfs along with 68% confidence limits on individual parameters. Most of the two-dimensional marginalized pdfs are relatively well determined. The distance is a factor of 2 higher than the DM distance, although this is not uncommon for pulsars out of the Galactic Plane (Roberts 2011; Kaplan et al. 2013). We do not have a strong constraint on the inclination other than $\cos i < 0.38$ at 95% confidence ($i > 68^\circ$). Even though the uncertainties on T_{night} and T_{day} overlap, there is actually a well-determined irradiation efficiency as T_{night} and T_{day} are highly correlated. The best-fit lightcurve is given in Figure 5.

To explore the effects of our assumptions for corotation and gravity darkening, we did a limited series of experiments. We tried a corotation factor of 0.5 (rotation at half of the orbital speed) and a gravity darkening factor $\beta = 0.04$. In both cases the majority of the fitted parameters remain within 1- σ of their nominal values. Only the filling factor changes slightly (still by $< 2\sigma$), and this is largely to keep the shape of the photometric variations similar.

5. LONG-TERM PHOTOMETRY

In Figure 8 we show the LINEAR, CRTS, PTF, P60 r' , and LCOGT r' photometry from 2003–2014. A secular evolution towards lower companion brightness is apparent in all surveys. We examined photometry from nearby stars of comparable brightness and found no long-term or phase-dependent trends.

To quantify this, we fit the data with an analytic model:

$$m(\phi) = m_0 + a_1 \cos 2\pi\phi + a_2 \cos 4\pi\phi + a_3 \cos 6\pi\phi + a_4 \sin 2\pi\phi + a_5 \sin 4\pi\phi \quad (2)$$

where $m(\phi)$ is the magnitude at orbital phase ϕ and ϕ is in the range $0 \rightarrow 1$. The coefficient a_1 is dominated by irradiation, a_2 is dominated by ellipsoidal modulation, and a_3 accounts for residual distortion. Of the sine coefficients, a_4 captures relativistic beaming and a_5 fits residual distortions.

We fit for each coefficient $m_0, a_1, a_2, a_3, a_4, a_5$ in each time bin in Figure 8 after normalizing the values of m_0 to the PTF R -band. Parameter agreement between the different instruments is acceptable, as indicated by the reasonable goodness of fit ($\chi^2/\text{dof} = 1004.5/981$). Table 4 lists the best fit parameters.

Figure 6 shows the time evolution of the best fit parameters. The most striking change is in the evolution of m_0 , which becomes systematically larger with time (i.e., the companion becomes fainter). The best-fit linear change is $\dot{m}_0 = 0.0131 \pm 0.0010 \text{ mag yr}^{-1}$.

We tested for possible evolution in the orbital period to ensure that phase mis-specification was not the source of the observed decline in m_0 . (The integrated statistical uncertainty from the radio ephemeris on the orbital phase is just 0.16 sec over our ten-year baseline.) The best fit to our data is consistent with no change in the orbital period; the 1- σ confidence limits are $-2.1 \times 10^{-10} < \dot{P}_{\text{orb}} < 2.8 \times 10^{-9}$. Additionally, if we discard all phase information and simply compute the median magnitudes in two-year bins, we see a comparable decline. We conclude that the observed dimming is

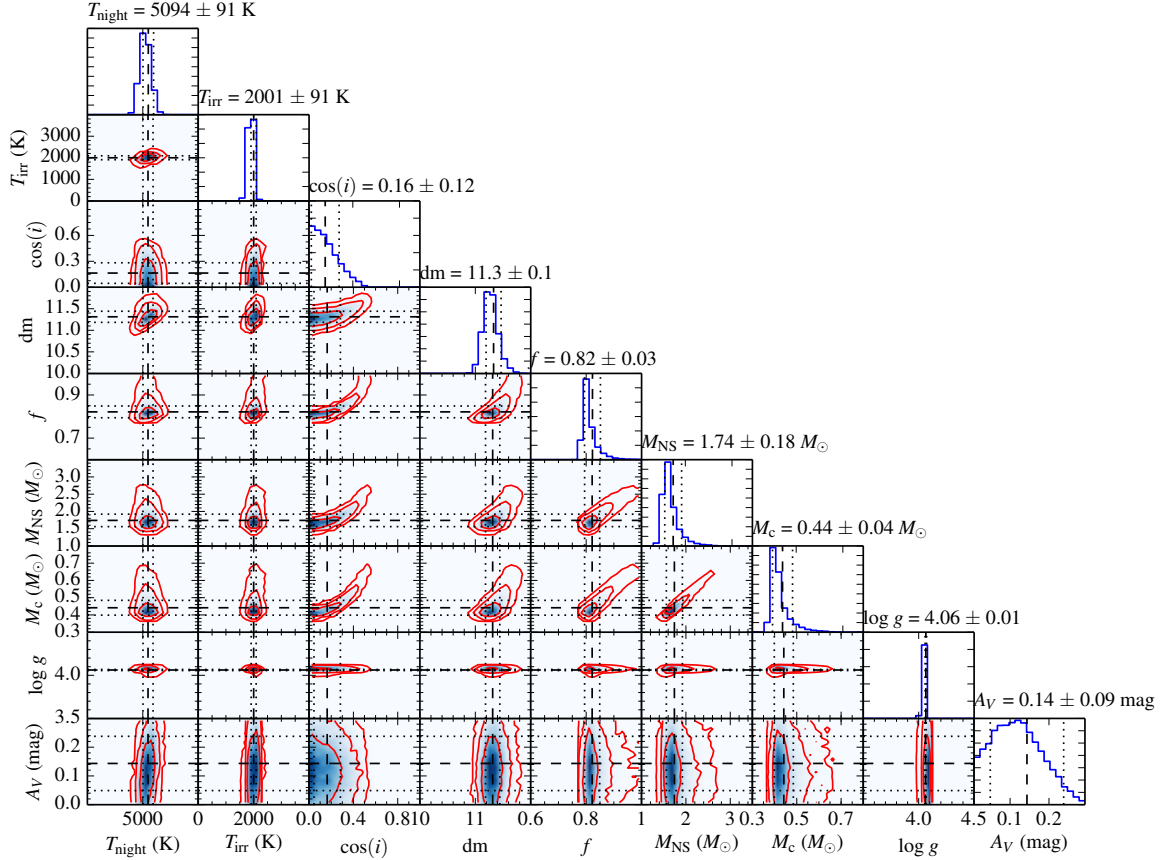


Figure 4. Joint two-dimensional posterior probability functions from the MCMC analysis. We show 1-, 2-, and 3- σ joint probability contours for each pair of parameters as well as the marginalized one-dimensional posterior pdfs for each parameter. See Table 3 for details.

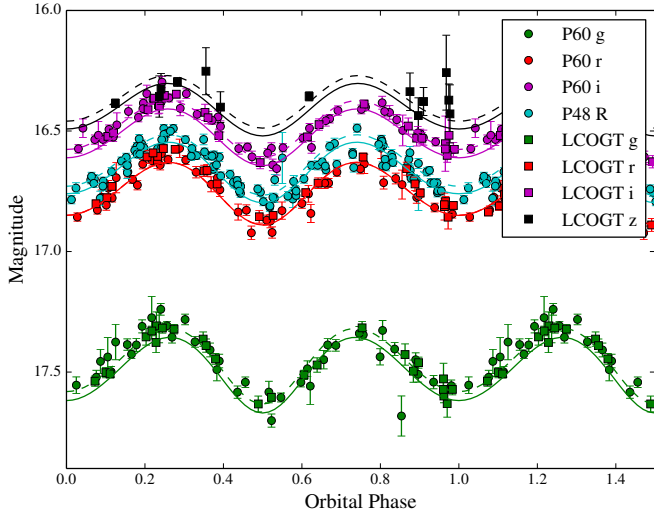


Figure 5. Best-fit lightcurve for PSR J2129–0429, using the P60, P48, and LCOGT photometry. The lightcurve is repeated 1.5 times for clarity. For each band we show the nominal model lightcurve (solid line) as well as the lightcurve with shifts to account for zero-point uncertainties (dashed line), all of which were < 0.04 mag.

robust to variations of the orbital period at this scale and assume $\dot{P}_{\text{orb}} = 0$ for the remaining discussion.

Despite the clear linear decline in m_0 , secular changes in the other coefficients are less apparent. Our ability to discern shape changes is hindered by the heterogeneous dataset, with instruments, phase coverage, and precision varying from year to year. Few of the linear fits to the

parameter evolution shown in Figure 6 are formally acceptable; χ^2 values for m_0 – a_5 are 45.9, 17.5, 8.0, 16.6, 25.8, and 3.0, all for 4 degrees of freedom. All of the coefficients except a_4 appear generally consistent with a constant value, but with one or two stochastically outlying points that we attribute to the mixed dataset.

The behavior the coefficient a_4 is particularly difficult to interpret. This sine term corresponds to relativistic beaming. For our fit radial velocity amplitude $K = 250 \text{ km s}^{-1}$, the expected amplitude is $\approx 4 \text{ mmag}$ (Loeb & Gaudi 2003). However, our fit values are nearly an order of magnitude larger and change sign, implying an physically impossible reversal of the orbital velocity. Moreover, the sine coefficient a_5 is inconsistent with the value of zero we would expect from a self-consistently modeled lightcurve (Mazeh & Faigler 2010).

We also fit Equation 2 to our best-fit binary model from § 4. In this case a_1 – a_3 took values very similar to those obtained from direct fits to the data, but a_4 and a_5 were approximately zero. This suggests that our fit values of a_4 and a_5 are modeling (possibly spurious) features of the data not present in the geometric approximation of the photosphere assumed by *Icarus*. These apparent shape variations are most likely due to the complexities of combining photometry with irregular phase coverage from several distinct surveys. More speculatively, however, it is possible that we are seeing an additional emission component from outside the companion’s Roche lobe—for example, from the intrabinary shock region, if the radio-eclipsing material there is not optically

Table 3
Best-fit Binary Parameter Values for PSR J2129–0429
Based on the MCMC Icarus Analysis

Parameter	Value
Fitted Parameters	
$\cos i^a$	0.16 \pm 0.12
T_{night}^b (K)	5094 \pm 90
T_{day}^c (K)	5124 \pm 92
K^d (km s $^{-1}$)	250.3 \pm 4.3
dm e	11.3 \pm 0.1
A_V^f (mag)	0.14 \pm 0.09
f^g	0.82 \pm 0.03
χ^2 / DOF	558.9 / 328
Derived Parameters	
d^h (pc)	1833 \pm 110
$\log(g)^i$	4.06 \pm 0.01
q^j	3.94 \pm 0.07
M_c^k (M_\odot)	0.44 \pm 0.04
M_{NS}^l (M_\odot)	1.74 \pm 0.18
i^m (deg)	80.5 \pm 7.0
T_{irr}^n (K)	2001 \pm 91
η^o (%)	3.0 \pm 0.6
R/R_L^p	0.95 \pm 0.01

^a Cosine of the inclination angle i .

^b Night-side temperature of the companion (i.e., the side facing away from the pulsar).

^c Day-side temperature of the companion (i.e., the side facing toward the pulsar).

^d Radial velocity amplitude of the companion.

^e Distance modulus.

^f V -band extinction.

^g Ratio of the radius of the companion pointing to the pulsar to that of the L1 point.

^h Distance.

ⁱ Volume-averaged surface gravity of the companion.

^j Mass ratio.

^k Companion mass.

^l Pulsar mass.

^m Inclination angle.

ⁿ Irradiation temperature, $(T_{\text{day}}^4 - T_{\text{night}}^4)^{1/4}$.

^o Irradiation efficiency, $4\pi a^2 \sigma T_{\text{irr}}^4 / \dot{E}$, where a is the semi-major axis.

^p Ratio of the volume-averaged radius to the volume-averaged Roche lobe radius.

thin. Roberts et al. (2015) report that the X-ray emission from PSR J2129–0429 shows an unusual phase dependence, with two strong but asymmetric peaks bracketing the companion superior conjunction, near the quadrature phases. Such a signal could put power into the a_4 and a_5 sine coefficients. On the other hand, our optical spectroscopy of the system does not display any features obviously distinct from a stellar companion.

We explored potential physical origins of the observed long-term variation of m_0 . For the companion to get fainter, we could have a change in the radius (becomes smaller), in the effective temperature (becomes cooler), or both. These could be due to perturbation by a past episode of active accretion that occurred before 2003, when our photometry begins. We tested these possibilities by modifying our best-fit binary models.

First, we changed the Roche filling factor (equivalent to changing the radius). As expected, as the filling factor decreases the companion gets fainter, with a fractional decrease of 0.01%/yr required to match

the change in m_0 . However, the other coefficients also changed (indeed, we would expect the ellipsoidal modulations to decrease as the filling factor decreases). The most significant change is in a_2 , which would change by $-0.003 \text{ mag yr}^{-1}$. As seen in Figure 6, a_2 is essentially constant except for the final bin. The best-fit line gives $\dot{a}_2 = -0.0007 \pm 0.0005 \text{ mag yr}^{-1}$, smaller than predicted under the assumption that the flux decline is due to the companion shrinking.

The other simple option would be a change in effective temperature. We decreased both the night-side (base) temperature and day-side temperatures, with the irradiation temperature fixed. This may be overly simplified, if the pulsar’s irradiation is changing, but our fits suggest the irradiation term a_1 is essentially constant. In this model the change in m_0 requires a decrease of about 10 K yr^{-1} in T_{night} , which also leads to a change in a_2 of $0.0001 \text{ mag yr}^{-1}$, only slightly smaller than the observed value. There is also a decrease in the mean $g - r$ color of $0.004 \text{ mag yr}^{-1}$. Since we only have a single epoch of well-sampled multi-band photometry we cannot look for color variations at this time.

While a decreasing effective temperature is most consistent with our current data, the thermal timescale of the star is 10 Myr, much longer than the yearly dimming we observe. Even when limited to the convective envelope, the thermal timescale is 3 Myr.

Despite the clear trend towards dimmer companion magnitudes seen in CRTS, LCOGT, and PTF, we are thus unable to form a self-consistent picture for the physical cause of the variation. Additional multicolor and high-SNR monitoring in the years ahead should help resolve this ambiguity.

6. DISCUSSION

While PSR J2129–0429 clearly meets the observational criteria for identification as a redback system—it is an eclipsing MSP with a nondegenerate companion of a few tenths of a solar mass—its extreme parameters relative to other systems in that population as well as its unusual position in evolutionary phase space make it unique among currently known redbacks.

Our best-fit mass for the non-degenerate companion of PSR J2129–0429 is $M_c = 0.44 \pm 0.04 M_\odot$, one of the heaviest of known redback systems. (PSR J1723–2837 may have a heavier companion, but its mass is poorly constrained ($0.4\text{--}0.7 M_\odot$; Crawford et al. 2013).) Combined with its long pulse period (7.6 msec; Hessels et al. 2011) and strong magnetic field ($B \sim 1.6 \times 10^9 \text{ G}$; Roberts et al. 2015) relative to other redback systems (Roberts 2013), these data suggest that the PSR J2129–0429 system is early in its recycling phase.

The pulsar companion is 95% Roche-lobe filling, consistent with a “quasi-Roche lobe overflow” (qRLOF) state where irradiation feedback during a previous accretion phase causes the companion to transfer more mass than it would without irradiation, leaving it just below Roche filling after the cessation of accretion (Benvenuto et al. 2015). As discussed in that paper, however, the qRLOF model cannot account for the \sim year timescale variations seen here as well as in the redback systems that have been observed to transition between accreting and detached states. While accretion disk instabil-

Years	m_0	a_1	a_2	a_3	a_4	a_5	χ^2	dof	χ^2_ν
2003-2004	16.545±0.003	0.004±0.005	0.114±0.004	-0.010±0.005	0.003±0.005	0.018±0.005	144.0	113	1.27
2005-2006	16.573±0.003	0.010±0.004	0.113±0.005	-0.013±0.004	-0.006±0.005	0.012±0.004	177.5	205	0.87
2007-2008	16.598±0.003	-0.001±0.004	0.117±0.004	0.001±0.005	0.013±0.005	0.021±0.005	211.7	184	1.15
2009-2010	16.637±0.002	-0.010±0.002	0.117±0.002	-0.014±0.002	-0.004±0.002	0.014±0.002	228.0	220	1.04
2011-2012	16.644±0.003	-0.004±0.004	0.117±0.003	-0.017±0.003	-0.022±0.003	0.015±0.004	127.4	142	0.90
2013-2014	16.680±0.002	-0.003±0.002	0.106±0.002	-0.005±0.003	-0.022±0.002	0.015±0.002	116.0	117	0.99
Total							1004.5	981	1.02

Table 4

Best-fit coefficients (Equation 2) for the photometric evolution of PSR J2129–0429 by year.

ities could account for the state changes in the transitioning systems, they are unlikely to be relevant for PSR J2129–0429.

The orbital period and companion mass of the PSR J2129–0429 system appear compatible with standard binary evolution of a neutron star and a normal main-sequence companion under some initial conditions (Figure 2 of Podsiadlowski et al. 2002). Interestingly, the bifurcation of evolutionary tracks into short and long period systems occurs near the position of PSR J2129–0429 in the $P_{\text{orb}}-M_c$ plane.

To explore the possible evolutionary history of PSR J2129–0429, we conducted a series of simulations using the Modules for Experiments in Stellar Astrophysics (MESA) code (Paxton et al. 2011, 2013, 2015). Figure 7 shows the evolutionary path of a $1.143 M_\odot$ zero-age main sequence donor orbiting a $1.6 M_\odot$ neutron star. We examined the effect of varying the initial orbital period in a range from 2.40 to 2.60 d. For these curves we assumed mass loss fractions in the vicinity of the donor and of the neutron star of $\alpha = 0.2$ and $\beta = 0.5$, respectively, thus resulting in an overall accretion efficiency by the neutron star $\epsilon = 0.2$. Effects of evaporation through irradiation were neglected for reasons that will become apparent later. Systems with initial orbital periods $\lesssim 2.50$ d are converging (case A evolution; Tauris & van den Heuvel 2006) and will evolve to become black widows and redbacks. At larger initial orbital separations, mass transfer only sets in on the red giant branch (case B evolution; Tauris & van den Heuvel 2006) and so these systems will diverge to become pulsar binaries with He-core white dwarf companions. At 2.50 d the PSR J2129–0429 system is marginally diverging, but angular momentum loss due to gravitational wave radiation eventually makes the orbit shrink once the main phase of mass transfer has stopped. Also displayed are evolutionary tracks for 2.50 d initial periods having different mass-loss parameters.

Given our observational constraints on companion mass, radius, and temperature as well as the orbital period, we can determine which evolutionary tracks are feasible by requiring that they produce consistent observables at a single age. As we can see, our evolution tracks indicate that the initial orbital period must be very close to the bifurcation period and require $\alpha \sim 0.25$, while the effect of β is negligible in the considered range of evolution. Changing the assumed initial mass ratio qualitatively only changes the timescale of the evolution.

For a reasonable range of initial neutron star masses, the evolution at a similar mass ratio remains unchanged, except for a rescaling of the initial orbital period. In the $M_{\text{NS},i} = 1.6 M_\odot$ scenario, the accreted mass is $\sim 0.2 M_\odot$

which implies a neutron star mass of $1.8 M_\odot$ which is similar to the value inferred from our light curve modeling. While we have not searched for compatible solutions for an exhaustive range for parameters at other mass ratios, we found that the mass ratio needs to be close to the presented one if $\alpha = 0.2$ and $\beta = 0.5$. In every case, we found that the only systems able to reproduce the observed properties are always close to the bifurcation period.

In light of our binary evolution work, we conclude that PSR J2129–0429 is in a very specific region of the phase space. At present the system is close to Roche-lobe filling and thus given its mass could not have been in a significantly tighter orbit in the past. Irradiation from the pulsar is very mild because of the large orbital separation and, despite the fact that it could have been larger in the past when the pulsar was spinning faster, it is unlikely that it has ever been very effective. Indeed, as demonstrated by Chen et al. (2013), evaporation through irradiation leads to an increase of the orbital period and so this mechanism could not have happened significantly given that the current orbit is close to the shortest separation that it has ever been. This also justifies our assumption to neglect the effect of irradiation.

The fate of PSR J2129–0429 is somewhat ambiguous as it lies right at the boundary between systems that will become redbacks/black widows and those that will widen and form a He-core white dwarf. Gravitational wave radiation should cause the system to shrink, but whether the orbit may become significantly compact within the next billion years or so depends on how further mass transfer and irradiation will operate. As it is, the orbit might well still be marginally widening if residual mass transfer is still operating.

Our modeling shows that it is possible to produce the observed high pulsar mass ($M_{\text{NS}} = 1.74 \pm 0.2 M_\odot$) with some assumptions under standard recycling scenarios. Other evolutionary scenarios are not ruled out, however. Production of a NS with this mass via Accretion Induced Collapse rather than recycling appears possible, but would require a rapidly-rotating WD and high accretion efficiency (Smedley et al. 2015). Another possibility is that the neutron star was born heavy, with a mass near the observed $1.74 M_\odot$ (Tauris et al. 2011).

The origin of the 13 mmag yr^{-1} dimming of the companion of PSR J2129–0429 discovered in this work remains uncertain. If the companion is shrinking, we would expect to see larger changes in the ellipsoidal modulation of the phased lightcurve than are observed. Cooling of the companion is compatible with these data, but the expected thermal timescales for the system are much longer than the observed yearly variations. Future multi-color

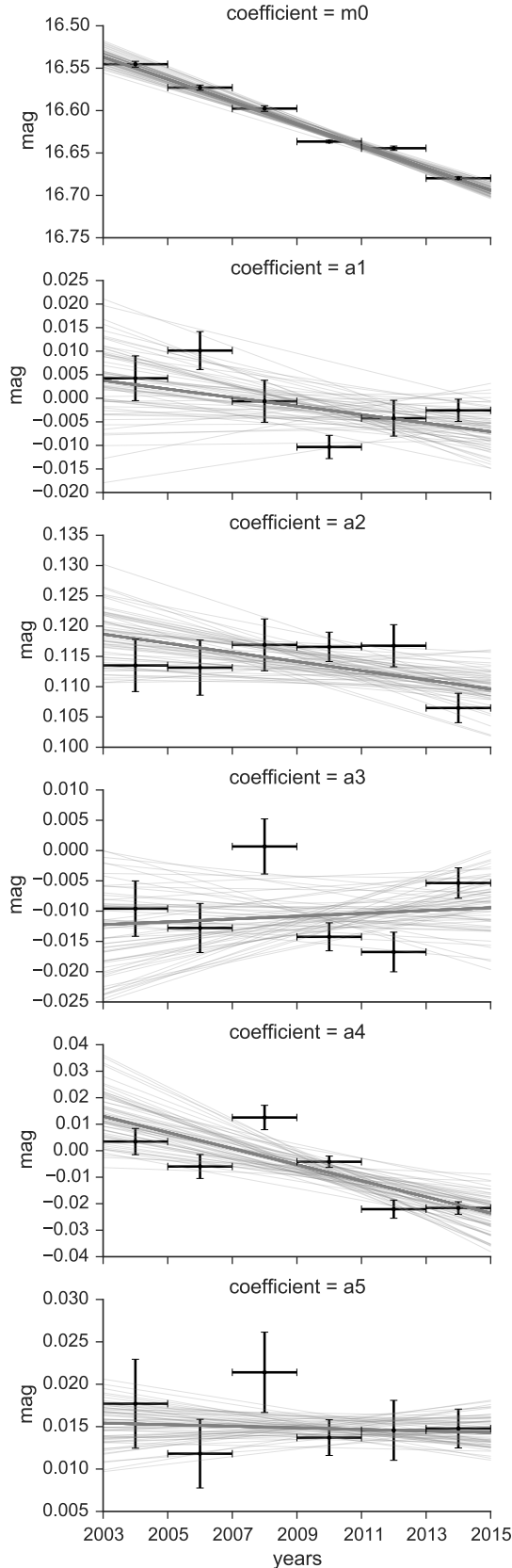


Figure 6. Temporal evolution of the best-fit lightcurve parameters (Equation 2). The dark gray lines are the best fit linear model; random deviates drawn from the fit covariance matrix are plotted in light gray.

observations will be valuable in monitoring the ongoing evolution of this unique system. Further investigation may reveal if PSR J2129–0429 will eventually destroy its companion or if—like the katipo spider found in New Zealand—it is a redback that shuns cannibalism.

T.A.P., E.C.B., and S.T. acknowledge partial support through NASA Grant No. NNX12AO76G. R.P.B. has received funding from the European Union Seventh Framework Programme under grant agreement PIFI-GA-2012-332393. J.W.T.H. acknowledges funding from an NWO Vidi fellowship and ERC Starting Grant “DRAGNET” (337062). E.C.B. and T.A.P. thank the Aspen Center for Physics and the NSF Grant #1066293 for hospitality during the editing of this paper.

This paper is based in part on observations obtained with the Palomar 48-inch Oschin telescope and the robotic Palomar 60-inch telescope at the Palomar Observatory as part of the Palomar Transient Factory project, a scientific collaboration among the California Institute of Technology, Columbia University, Las Cumbres Observatory, the Lawrence Berkeley National Laboratory, the National Energy Research Scientific Computing Center, the University of Oxford, and the Weizmann Institute of Science; and the Intermediate Palomar Transient Factory project, a scientific collaboration among the California Institute of Technology, Los Alamos National Laboratory, the University of Wisconsin, Milwaukee, the Oskar Klein Center, the Weizmann Institute of Science, the TANGO Program of the University System of Taiwan, and the Kavli Institute for the Physics and Mathematics of the Universe.

The CSS survey is funded by the National Aeronautics and Space Administration under Grant No. NNG05GF22G issued through the Science Mission Directorate Near-Earth Objects Observations Program. The CRTS survey is supported by the U.S. National Science Foundation under grants AST-0909182, AST-1313422, and AST-1413600.

This work makes use of observations from the Las Cumbres Observatory Global Telescope Network.

Facilities: Hale (Double Beam Spectrograph), PO:1.2m (Palomar Transient Factory), PO:1.5m, LIN-EAR, CSS, LCOGT

REFERENCES

- Abdo, A. A., Ackermann, M., Ajello, M., et al. 2010, *ApJS*, 188, 405
 Ackermann, M., Ajello, M., Allafort, A., et al. 2012, *ApJ*, 753, 83
 Alam, S., Albareti, F. D., Allende Prieto, C., et al. 2015, *ApJS*, 219, 12
 Alpar, M. A., Cheng, A. F., Ruderman, M. A., & Shaham, J. 1982, *Nature*, 300, 728
 Antoniadis, J., Freire, P. C. C., Wex, N., et al. 2013, *Science*, 340, 448
 Archibald, A. M., et al. 2009, *Science*, 324, 1411
 Bailes, M., Bates, S. D., Bhalariao, V., et al. 2011, *Science*, 333, 1717
 Bassa, C. G., van Kerkwijk, M. H., Koester, D., & Verbunt, F. 2006, *A&A*, 456, 295
 Bassa, C. G., Patruno, A., Hessels, J. W. T., et al. 2014, *MNRAS*, 441, 1825
 Benvenuto, O. G., De Vito, M. A., & Horvath, J. E. 2014, *ApJ*, 786, L7
 —. 2015, *ApJ*, 798, 44

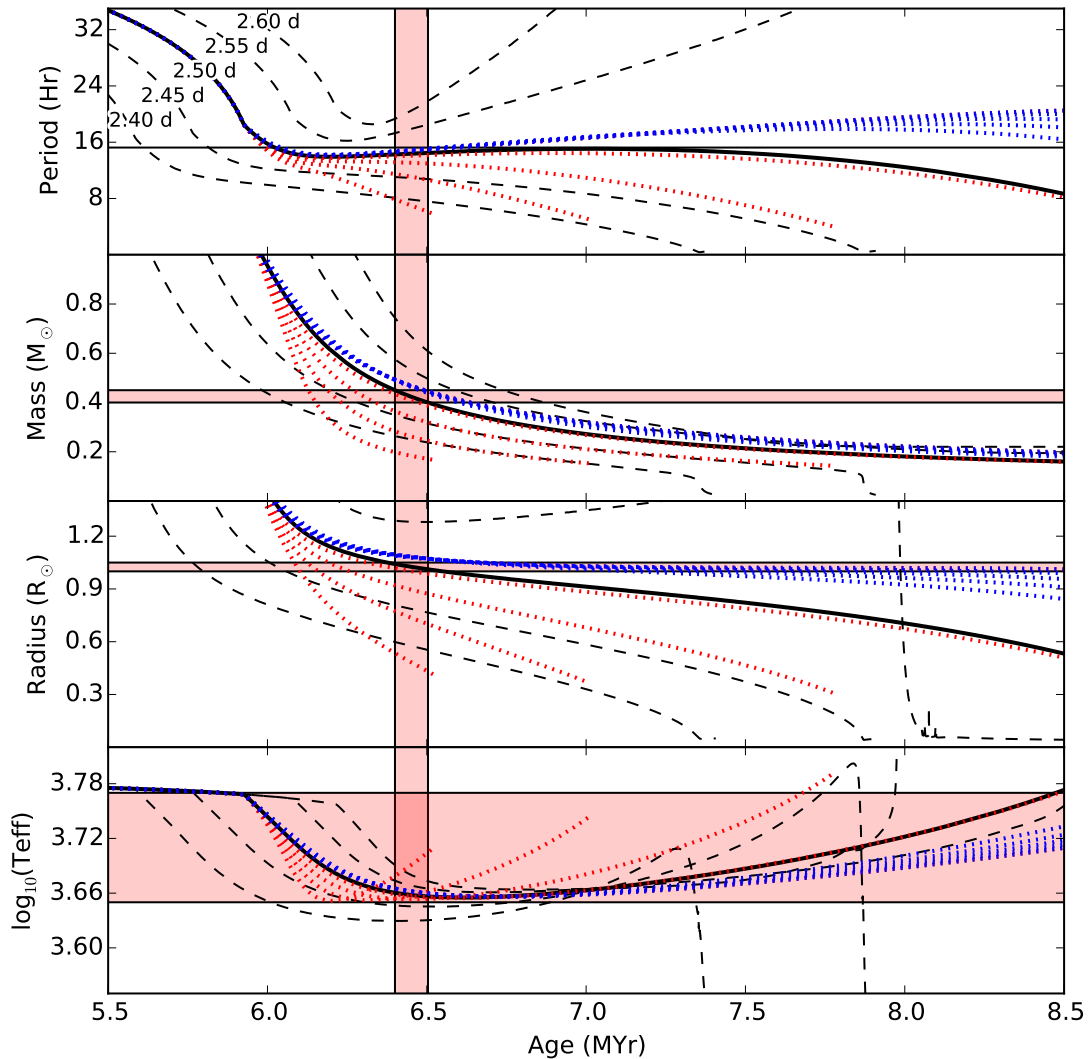


Figure 7. The evolutionary path of the orbital period, donor mass, donor radius, and donor temperature for a $1.143 M_{\odot}$ zero-age main sequence donor orbiting a $1.6 M_{\odot}$ neutron star. The solid lines display the effect of varying the initial orbital period in a range from 2.40 to 2.60 d. The dotted lines show the effects of varying mass loss assuming the 2.50 d initial period. The blue dotted lines display the effect of mass loss at the companion, with $\alpha = 0$ and $\beta = 0, 0.25, 0.5, 0.75, 1$, from top to bottom. The red dotted lines display the effect of mass loss at the neutron star, with $\beta = 0$ and $\alpha = 0, 0.25, 0.5, 0.75, 1$, from top to bottom. Note that the uppermost blue and red lines (e.g. $\alpha, \beta = 0$) overlap. On each plot, the horizontal red shaded region represents the 68% probability of the given parameter as inferred from our optical light curve modeling. The vertical red shaded region corresponds to the age compatible with the companion mass for the 2.50 d model.

- Bertin, E., & Arnouts, S. 1996, *A&AS*, 117, 393
 Bhalerao, V. B., van Kerkwijk, M. H., & Harrison, F. A. 2012, *ApJ*, 757, 10
 Bhattacharya, D., & van den Heuvel, E. P. J. 1991, *Phys. Rep.*, 203, 1
 Board, I. S. 2015, IAU SOFA Software Collection
 Breton, R. P., van Kerkwijk, M. H., Roberts, M. S. E., et al. 2013, *ApJ*, 769, 108
 Cenko, S. B., Fox, D. B., Moon, D.-S., et al. 2006, *PASP*, 118, 1396
 Chen, H.-L., Chen, X., Tauris, T. M., & Han, Z. 2013, *ApJ*, 775, 27
 Cordes, J. M., & Lazio, T. J. W. 2002, *ArXiv Astrophysics e-prints*, astro-ph/0207156
 Crawford, F., Lyne, A. G., Stairs, I. H., et al. 2013, *ApJ*, 776, 20
 Deller, A. T., Archibald, A. M., Brisken, W. F., et al. 2012, *ApJ*, 756, L25
 Deloye, C. J., & Bildsten, L. 2003, *ApJ*, 598, 1217
 Demorest, P. B., Pennucci, T., Ransom, S. M., Roberts, M. S. E., & Hessels, J. W. T. 2010, *Nature*, 467, 1081
 Drake, A. J., Djorgovski, S. G., Mahabal, A., et al. 2009, *ApJ*, 696, 870
 Drake, A. J., Graham, M. J., Djorgovski, S. G., et al. 2014, *ApJS*, 213, 9
 Freire, P. C. C., Bassa, C. G., Wex, N., et al. 2011, *MNRAS*, 412, 2763
 Fruchter, A. S., & Goss, W. M. 1992, *ApJ*, 384, L47
 Fruchter, A. S., Stinebring, D. R., & Taylor, J. H. 1988, *Nature*, 333, 237
 Hessels, J. W. T., Roberts, M. S. E., McLaughlin, M. A., et al. 2011, in *American Institute of Physics Conference Series*, Vol. 1357, American Institute of Physics Conference Series, ed. M. Burgay, N. D’Amico, P. Esposito, A. Pellizzoni, & A. Possenti, 40
 Kaplan, D. L., Bhalerao, V. B., van Kerkwijk, M. H., et al. 2013, *ApJ*, 765, 158

- King, A. R., Davies, M. B., & Beer, M. E. 2003, *MNRAS*, 345, 678
- Kluzniak, W., Ruderman, M., Shaham, J., & Tavani, M. 1988, *Nature*, 334, 225
- Laher, R. R., Surace, J., Grillmair, C. J., et al. 2014, *PASP*, 126, 674
- Lattimer, J. M. 2012, *Annual Review of Nuclear and Particle Science*, 62, 485
- Law, N. M., Kulkarni, S. R., Dekany, R. G., et al. 2009, *PASP*, 121, 1395
- Levinson, A., & Eichler, D. 1991, *ApJ*, 379, 359
- Li, M., Halpern, J. P., & Thorstensen, J. R. 2014, *ApJ*, 795, 115
- Loeb, A., & Gaudi, B. S. 2003, *ApJ*, 588, L117
- Lucy, L. B. 1967, *ZAp*, 65, 89
- Mazeh, T., & Faigler, S. 2010, *A&A*, 521, L59
- Munari, U., Sordo, R., Castelli, F., & Zwitter, T. 2005, *A&A*, 442, 1127
- Nice, D. J., Splaver, E. M., Stairs, I. H., et al. 2005, *ApJ*, 634, 124
- Nolan, P. L., Abdo, A. A., Ackermann, M., et al. 2012, *ApJS*, 199, 31
- Ofek, E. O., Frail, D. A., Breslauer, B., et al. 2011, *ApJ*, 740, 65
- Ofek, E. O., Laher, R., Law, N., et al. 2012, *PASP*, 124, 62
- Oke, J. B., & Gunn, J. E. 1982, *PASP*, 94, 586
- Papitto, A., Ferrigno, C., Bozzo, E., et al. 2013, *Nature*, 501, 517
- Patruno, A., Archibald, A. M., Hessels, J. W. T., et al. 2014, *ApJ*, 781, L3
- Paxton, B., Bildsten, L., Dotter, A., et al. 2011, *ApJS*, 192, 3
- Paxton, B., Cantiello, M., Arras, P., et al. 2013, *ApJS*, 208, 4
- Paxton, B., Marchant, P., Schwab, J., et al. 2015, *ArXiv e-prints*, [arXiv:1506.03146](https://arxiv.org/abs/1506.03146) [[astro-ph.SR](https://arxiv.org/abs/1506.03146)]
- Phinney, E. S., Evans, C. R., Blandford, R. D., & Kulkarni, S. R. 1988, *Nature*, 333, 832
- Phinney, E. S., & Kulkarni, S. R. 1994, *ARA&A*, 32, 591
- Podsiadlowski, P., Rappaport, S., & Pfahl, E. D. 2002, *ApJ*, 565, 1107
- Radhakrishnan, V., & Srinivasan, G. 1982, *Current Science*, 51, 1096
- Rahmer, G., Smith, R. M., Bui, K., et al. 2012, in *Society of Photo-Optical Instrumentation Engineers (SPIE) Conference Series*, Vol. 8446, *Society of Photo-Optical Instrumentation Engineers (SPIE) Conference Series*, 2
- Rau, A., Kulkarni, S. R., Law, N. M., et al. 2009, *PASP*, 121, 1334
- Roberts, M. S. E. 2011, in *AIP Conf. Ser.*, Vol. 1357, *Radio Pulsars: An Astrophysical Key to Unlock the Secrets of the Universe*, ed. M. Burgay, N. D'Amico, P. Esposito, A. Pellizzoni, & A. Possenti, 127
- Roberts, M. S. E. 2013, in *IAU Symposium*, Vol. 291, *IAU Symposium*, ed. J. van Leeuwen, 127
- Roberts, M. S. E., McLaughlin, M. A., Gentile, P. A., et al. 2015, *ArXiv e-prints*, [arXiv:1502.07208](https://arxiv.org/abs/1502.07208) [[astro-ph.HE](https://arxiv.org/abs/1502.07208)]
- Romani, R. W., Filippenko, A. V., Silverman, J. M., et al. 2012, *ApJ*, 760, L36
- Schlafly, E. F., & Finkbeiner, D. P. 2011, *ApJ*, 737, 103
- Schroeder, J., & Halpern, J. 2014, *ApJ*, 793, 78
- Sesar, B., Stuart, J. S., Ivezić, Z., et al. 2011, *AJ*, 142, 190
- Sesar, B., Grillmair, C. J., Cohen, J. G., et al. 2013, *ApJ*, 776, 26
- Smedley, S. L., Tout, C. A., Ferrario, L., & Wickramasinghe, D. T. 2015, *MNRAS*, 446, 2540
- Stappers, B. W., Archibald, A. M., Hessels, J. W. T., et al. 2014, *ApJ*, 790, 39
- Stokes, G. H., Evans, J. B., Vighh, H. E. M., Shelly, F. C., & Pearce, E. C. 2000, *Icarus*, 148, 21
- Strader, J., Chomiuk, L., Cheung, C. C., et al. 2015, *ArXiv e-prints*, [arXiv:1502.05999](https://arxiv.org/abs/1502.05999) [[astro-ph.HE](https://arxiv.org/abs/1502.05999)]
- Tauris, T. M., Langer, N., & Kramer, M. 2011, *MNRAS*, 416, 2130
- Tauris, T. M., & van den Heuvel, E. P. J. 2006, *Formation and evolution of compact stellar X-ray sources*, ed. W. H. G. Lewin & M. van der Klis, 623
- The Fermi-LAT Collaboration. 2015, *ArXiv e-prints*, [arXiv:1501.02003](https://arxiv.org/abs/1501.02003) [[astro-ph.HE](https://arxiv.org/abs/1501.02003)]
- Tody, D. 1986, in *Society of Photo-Optical Instrumentation Engineers (SPIE) Conference Series*, Vol. 627, *Instrumentation in astronomy VI*, ed. D. L. Crawford, 733
- van den Heuvel, E. P. J., & van Paradijs, J. 1988, *Nature*, 334, 227
- van Kerkwijk, M. H., Breton, R. P., & Kulkarni, S. R. 2011, *ApJ*, 728, 95
- York, D. G., Adelman, J., Anderson, Jr., J. E., et al. 2000, *AJ*, 120, 1579

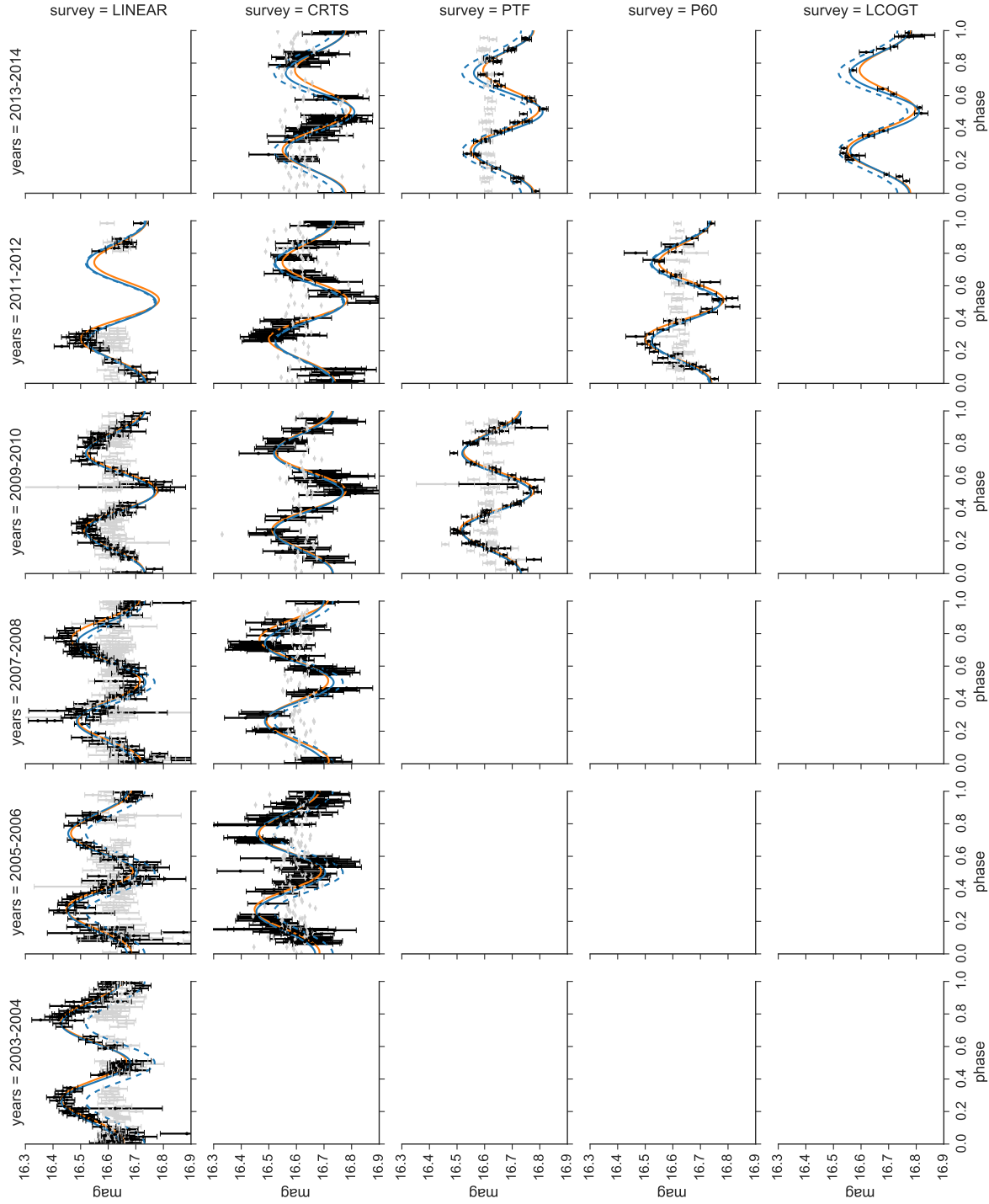


Figure 8. Long-term photometry for PSR J2129–0429 from LINEAR, CRTS, PTF, P60 (r'), and LCOGT (r'). Data are grouped in two-year intervals. Orbital phases are computed from the radio ephemeris. Photometry of PSR J2129–0429 is shown in black, while that of the nearby comparison star is shown in grey. Errors on the CRTS companion photometry are omitted for clarity but are comparable to that of the pulsar. We fit and removed constant offsets from LINEAR (-0.82 mag), CRTS (-0.08 mag), P60 (-0.11 mag), and LCOGT (-0.11 mag) to match PTF. Model fits by year with fixed sine and cosine amplitudes are shown in solid blue lines, while the fit to the 2009–2010 data is replicated in blue dashed lines to illustrate the temporal evolution of the source. Model fits by year with the sine and cosine amplitudes free to vary are plotted in orange.